Modelling of Mechanical Properties for Integrated Casting and Rolling Processes Using Dedicated Extra-High Temperature Solutions Platform

Marcin Hojny
Dept. of Applied Computer Science and Modelling
AGH University of Science and Technology
A. Mickiewicza Av. 30, 30-059 Kraków, Poland
e-mail: mhojny@metal.agh.edu.pl

Miroslaw Glowacki
Dept. of Applied Computer Science and Modelling
AGH University of Science and Technology
A. Mickiewicza Av. 30, 30-059 Kraków, Poland
e-mail: glowacki@metal.agh.edu.pl

***Abstract*—The main subject of the current paper is the modelling of mechanical properties of carbon steels at a temperature which exceeds the typical hot rolling temperature range as well as a new methodology of such investigation was developed. The method requires high accuracy model of semi-solid steel deformation. Hence, it requires a dedicated hybrid analytical-numerical model of deformation of steel with variable density. The newly developed methodology allows to compute curves depending on both temperature and strain rate. In aim to verify the new modified methodology, a number of experimental tests using Gleeble 3800 thermo-mechanical simulator were done. The comparison between numerical and experimental results are presented in the first part of the paper. The developed methodology allows reliable numerical simulation of deformation of semi-solid steel samples and calculation of realistic flow curve parameters. In the second part of the paper, the newest results of mechanical properties prediction of 11SMn30 grade steel as well as an example numerical and experimental results are presented.**

Keywords-strain-stress curve; semi-solid steel testing; extra-high deformation temperature; numerical analysis; inverse method

I. INTRODUCTION

Due to the global energy crisis in recent years, more and more new production technologies require energy preservation and environmental protection. The integrated casting and rolling technologies are newest efficient and very profitable ways of hot strip production. Only few companies all over the world are able to manage such processes. The technical staff of a plant located in Cremona, Italy is working on new methods of flat steel manufacturing for several years now. The ISP (Inline Strip Production) and AST (Arvedi Steel Technologies) technologies, which are developed in Cremona, are distinguished by very high rolling temperature. The main benefits of both methods are related to very low rolling forces and favourable field of temperature. However, certain problems particular to such metal treatment arise. The central parts of slabs are mushy and the solidification is not yet finished while the deformation is in progress. This results in changes in material density and occurrence of characteristic temperatures having great influence on the plastic behaviour of the material [1] [2] [3] [4] [5]. The nil strength temperature (NST), strength recovery temperature (SRT), nil ductility temperature (NDT) and ductility recovery temperature (DRT) have effect on steel plastic behaviour and limit plastic deformation [5]. The nil strength temperature (NST) is the temperature level at which material strength drops to zero, while the steel is being heated above the solidus temperature. Another temperature associated with NST is the strength recovery temperature (SRT). At this temperature the cooled material regains strength greater than 0.5 N/mm^2. Nil ductility temperature (NDT) represents the temperature at which the heated steel loses its ductility. The ductility recovery temperature (DRT) is the temperature at which the ductility of the material (characterised by reduction of area) reaches 5% while it is being cooled. Over this temperature, the plastic deformation is not allowed at any stress tensor configuration.

The most important steel property having crucial influence on metal flow paths is the yield stress. In the literature of the past years, one can find papers regarding experimental results [6] and modelling [7] of non-ferrous metals. Both the mentioned contributions focus mainly on tixotrophy. Thixoforming process is one member of a family of semi-solid forming processes and it possesses characteristics of both casting and forging. The first results regarding steel deformation at extra high temperature were only presented in the past few years [8]. This stems from the fact that level of liquidus and solidus temperatures of steel is very high in comparison with non-ferrous metals. It causes serious experimental problems contrary to deformation tests for non-ferrous metals which are much easier. Rising abilities of thermo-mechanical simulators such as the Gleeble 3800 and development of new methods of identification of mechanical properties allow investigations leading to strain-stress relationships for semi-solid steels, as well. This problem became a subject of research done by authors of the presented paper for several years now. As a result a computer system supporting the investigation of mushy steel has been developed. The current paper presents the modified methodology, which allows the calculation of

2013, © Copyright by authors, Published under agreement with IARIA - www.iaria.org

the real stress-strain relationships for a wide range of temperatures and strain rate. In Section II, the modified methodology of stress-strain curves is described. Section III presents a mathematical model, while Section IV presents experimental verification of the developed methodology. In Section V, the newest results of strain-stress prediction for simulations of rolling process are presented. Finally, in the last section, the main conclusions and future work are shortly described.

II. THE NEW METHODOLOGY

The old version of steel examination methodology, denoted as variant no. 1, was based on both tension and compression tests [12] [13]. The temperature range was divided into two sub-ranges: lower – below NDT – and higher – above this temperature. The usual experimental procedure based on tensile tests, which is valid for cold and low-level hot deformation was applied for the lower temperature range. The resulting yield curves were described by modified Voce formula using approximation of experimental data [11].

A special technique of testing was developed for temperatures higher than NDT due to several serious experimental problems. The deformation process has been divided into two main stages. The first one – a very small preliminary compression and the second one – the ultimate compression. The preliminary deformation was designed to eliminate clearances in the testing equipment. The coefficients of the Voce formula were calculated using inverse solutions. This was the only acceptable method due to strong strain inhomogeneity of semi-sold steel. This approach allowed to compute strain-stress curves depending on only one additional parameter – the temperature. The newly developed methodology (denoted as variant no. 2) allows the computation of curves depending on both temperature and strain rate. The tension tests has been replaced by compression ones and the Voce formula was replaced by more adequate equation. Contrary to the old version of the method the newly developed one allows the computation of curves depending on both temperature and strain rate. Figure 1 schematically presents the modified methodology. More details concerning the experimental work were published in [14]. The presented approach allows to compute realistic yield stress curves depending on strain, temperature and strain rate in temperature range from 1200°C to NDT and above. The objective function of the inverse analysis was defined as a square root error of discrepancies between calculated (F_c) and measured (F_m) loads at several subsequent steps of the compression process. The experimental values of the deformation forces were collected by the Gleeble 3800 equipment while the theoretical ones (F_c) were calculated with the help of a sophisticated solver facilitating accurate computation of strain, stress and temperature fields for materials with variable density.

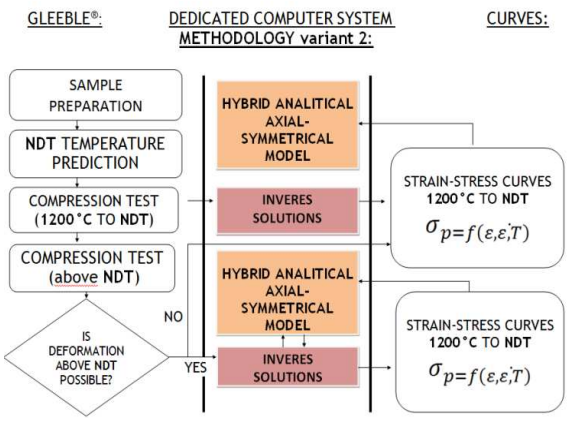

Figure 1. Flowchart of the integrated testing methodology of flow stress investigation of semi-solid steel.

This solver is the least visible but the most powerful part of the computer aided testing system developed by the authors called Def_Semi_Solid. The heart of the solver is based on a hybrid analytical-numerical mushy steel deformation model described in the next section. The Def_Semi_Solid solver was included into Extra-High Temperature Solutions Platform (EHTS Platform) in order to support modelling of plastic deformation of materials at very high temperature levels (Figure 2). The solutions platform consists of two independent tools: Def_Semi_Solid v.5.0 – complete 2D modelling toolset dedicated for Gleeble® 3800 thermo-mechanical simulator with integrated Pre&Postprocessor and DEFFEM 3D – vertical application toolset including three modules: DEFFEM solver (still in development) full three dimensional multiscale thermo-mechanical solver for new methodology purposes, DEFFEM inverse and DEFFEM pre&postprocessor. The last two modules were tested in real industrial tests during modelling of TIG welding process of Inconel super alloy and stamping processes. Those modules supported of boundary condition identification as well as strain-stress curves based on industrial results. More details concerning modelling of mentioned processes with DEFFEM inverse module support can be found in [9] [10] [15].

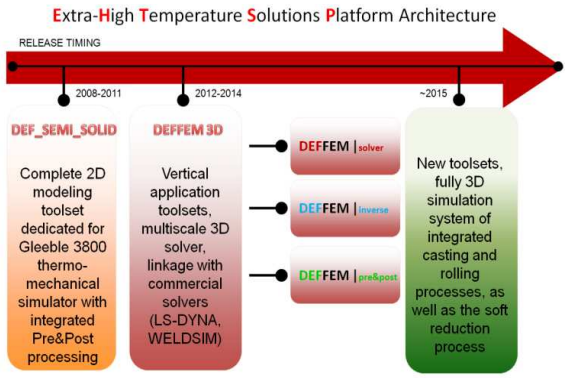

Figure 2. Architecture of extra-high temperature solutions platform.

2013, © Copyright by authors, Published under agreement with IARIA - www.iaria.org

The newest version of Def_Semi_Solid system is equipped with full automatic installation unit (Figure 3) and new graphical interface. It allows the computer aided testing of mechanical properties of steels at very high temperature using Gleeble 3800 physical simulators to avoid problems which arise by traditional testing procedures. The first module allows the establishment of new projects or working with previously existing ones (Figure 4). The integral parts of each project are: input data for a specific compression/tension test as well as the results of measurements and optimization. In the current version of the program the module permits application of a number of database engines (among other standard MSAcces, dBASE IV and Paradox 7-8 for PC-based systems) and allows the implementation of material databases and procedures of automatic data verification. The next module (the solver) gives user the possibility of managing the working conditions of the simulation process. The inverse analysis can be turned off or on using this part of the system.

Figure 3. The main window of the newest version of Def_Semi_Solid system.

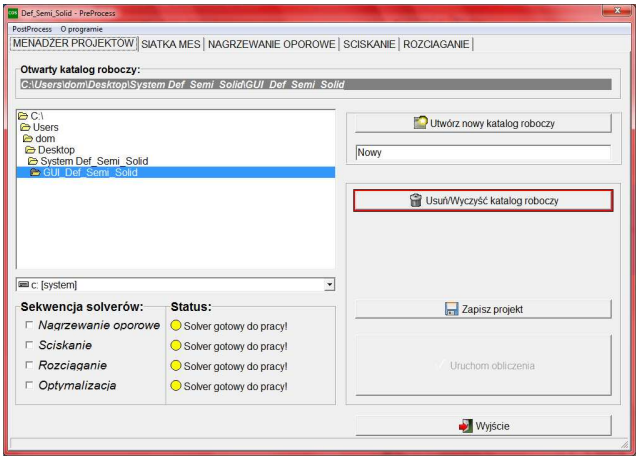

Figure 4. The Pre-processor of the newest version of Def_Semi_Solid system.

The last module (DSS/Post module) is dedicated to the visualisation of the numerical results and printing the final reports. In the current version the possibility of visualization was significant improved. The main are: shading options using OpenGL mode (2D and 3D) as shown in Figure 5 and possibility make a full contour map (2D and 3D) as shown in Figure 6.

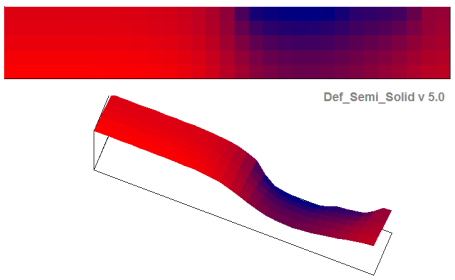

Figure 5. The Post-processor of the newest version of Def_Semi_Solid system (shading option 2D and 3D).

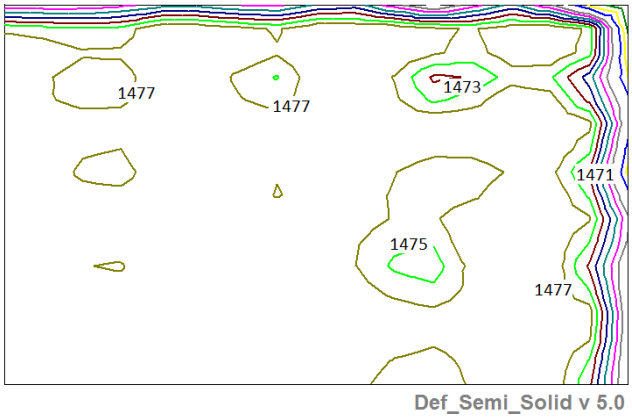

Figure 6. The Post-processor of the newest version of Def_Semi_Solid system (contour option).

III. MATHEMATICAL MODEL

A mathematical model of the compression process has been developed using the theory of plastic flow [11]. The principle of the upper assessment, calculus of variations, approximation theory, optimization and numerical methods for solving partial differential equations were used [16]. The following assumptions were established:

- Deformation and stress state are axial-symmetrical;
- Deformed material is isotropic but inhomogeneous;
- The material behaviour is rigid-plastic – the relationship between the stress tensor and strain rate tensor is calculated according to the Levy-Mises flow law [11], which is given as:

$$\sigma_{ij} - \frac{1}{3}\sigma_{kk}\delta_{ij} = \frac{2}{3}\frac{\sigma_p}{\dot{\varepsilon}_i}\dot{\varepsilon}_{ij} \quad (1)$$

2013, © Copyright by authors, Published under agreement with IARIA - www.iaria.org

Rigid-plastic model was selected due to its very good accuracy at the strain field during the hot deformation and sufficient correctness of calculated deviatoric part of the stress field. Moreover, the elastic part of each stress tensor component is very low at temperatures close to solidus line and can in practice be neglected in calculations of strain distribution. The limits for plastic metal behaviour are defined according to Huber-Mises-Hencky yield criterion:

$$\sigma_{ij}\sigma_{ij} = 2\left(\frac{\sigma_p}{\sqrt{3}}\right)^2 \quad (2)$$

In (1) and (2), σ_{ij} denotes the stress tensor components, σ_{kk} represents the mean stress, δ_{ij} is the Kronecker delta [11], σ_p indicates the yield stress, $\dot{\varepsilon}_i$ is the effective strain rate, and $\dot{\varepsilon}_{ij}$ denotes strain rate tensor components. The components are given by an equation:

$$\dot{\varepsilon}_{ij} = \frac{1}{2}\left(\nabla_i v_j + \nabla_j v_i\right) \quad (3)$$

In cylindrical coordinate system $Or\theta z$ the solution is a vector velocity field defined by the distribution of three coordinates $\boldsymbol{v} = (v_r, v_\theta, v_z)$. The field is a result of optimization of a power functional, which can be written in general form as the sum of power necessary to run the main physical phenomena related to plastic deformation. Due to the axial-symmetry of the sample the circumferential component of the velocity field can be neglected and the functional is usually formulated as:

$$J[\boldsymbol{v}] = \dot{W} = \dot{W}_\sigma + \dot{W}_\lambda + \dot{W}_f \quad (4)$$

Component $\dot{W}_\sigma$ occurring in (4) represents the plastic deformation power, $\dot{W}_\lambda$ is the power which is a penalty for the departure from mass conservation condition, $\dot{W}_f$ denotes the friction power and $\boldsymbol{v} = (v_r, v_z)$ describes the reduced velocity field distribution.

Rigid-plastic formulation of metal deformation problem requires the condition of mass conservation in the deformation zone. In case of solids and liquids with a constant density, this condition can be simplified to the incompressibility condition. Such a condition is generally satisfied with sufficient accuracy during the optimization of functional (4). In most solutions a slight, but noticeable loss of volume is observed. The loss occurs because the incompressibility condition imposed on the solution is not completely satisfied in numerical form. It is negligible in case of traditional computer simulation of deformation processes although in some embodiments more accurate methods are used to restore the volume of metal subjected to the deformation. In contrast, in the presented case the density of semi-solid materials varies during the deformation process and these changes result in a physically significant change in the volume of a body having constant mass. The size of the volume loss due to numerical errors is comparable with changes caused by fluctuation in the density of the material.

A further problem specific to the variable density continuum is power $\dot{W}_\lambda$, which occurs in functional (4). It is used in most solutions and has a significant share of total power. Even when the iterative process approaches the end, this power component is still significant, especially if the convergence of the optimization procedures is insufficient. In case of discretization of the deformation area (e.g., using the finite element method) if one focuses solely on the $\dot{W}_\lambda$ a number of possible locally optimal solutions appear. They are related to a number of possible directions of movement of discretization nodes providing the volume preservation of the deformation zone. Each of these solutions creates a local optimum for $\dot{W}_\lambda$ power and thus for the entire functional (4). This makes it difficult to optimize because of lack of uniform direction of fall of total power which leads to global optimum. The material density fluctuation causes further optimization difficulties, resulting from additional replacement of incompressibility condition with a full condition of mass conservation.

The proposed solution requires high accuracy in ensuring the incompressibility condition for the solid material or mass conservation condition for the semi-solid areas. This stems from the fact that the errors resulting from the breach of these conditions can be treated as a volume change caused by the steel density variation in the semi-solid zone. High accuracy solution is required also due to large differences in yield stress for the individual subareas of the deformation zone. In the discussed temperature range they appear due to even slight fluctuations in temperature. In presented solution the second component of functional (4) is left out and mass conservation condition is given in analytical form constraining the radial (v_r) and longitudinal (v_z) velocity field components. The functional takes the following shape:

$$J[\boldsymbol{v}] = \dot{W}_\sigma + \dot{W}_t \quad (5)$$

In case of functional (5), the numerical optimisation procedure converges faster than the one for functional (4) due to the reduced number of velocity field parameters (only radial components are optimisation parameters) and the lack of numerical form of mass conservation condition. The accuracy of the proposed hybrid solution is higher also due to negligible volume loss caused by numerical errors, which is very important for materials with variable density.

As mentioned before, the solution of the problem is a velocity field in cylindrical coordinate system in axial-symmetrical state of deformation. Optimization of metal flow velocity field in the deformation zone of semi-variational problem requires the formulation according to equation (5). The radial velocity distribution $v_r(r, \theta, z)$ and the longitudinal one $v_z(r, \theta, z)$ are so complex that such wording in the global coordinate system poses considerable difficulties. These difficulties are the result of the mutual dependence of these velocities. Therefore, the basic formulation will be written for the local cylindrical coordinate system $Or\theta z$ with a view to the future discretization of deformation area using one of the dedicated methods. In addition, one will find that the deformation of

2013, © Copyright by authors, Published under agreement with IARIA - www.iaria.org

cylindrical samples is characterized by axial symmetry. As demonstrated by experimental studies conducted using semi-solid samples the symmetry may be disturbed only as a result of unexpected leakage of liquid phase [16].

Such experiments, however, are regarded as unsuccessful and not subject to numerical analysis. Establishment of the axial symmetry, with the exception of cases of physical instability can be considered valid also for the process of compression or tensile test of semi-solid samples, allows one to simplify the model because of the identical strain distribution at any axial sample cross-section. Therefore, considerations will be carried out in Orz coordinates for the sample cross-section using one of the planes containing the sample axis. Components of power functional given by (5) have been formulated in accordance with the general theory of plasticity by relevant equations. The plastic power for the deformation zone having volume of V is given by the subsequent relation:

$$\dot{W}_\sigma = \int_V \sigma_i \dot{\varepsilon}_i \, dV \tag{6}$$

where σ_i is the effective stress and $\dot{\varepsilon}_i$ denotes the effective strain. The plastic deformation starts when the rising effective stress reaches yield stress limit σ_p ($\sigma_i = \sigma_p$) according to yield criterion given by equation (2). Effective strain occurring in (6) is calculated on the basis of the strain tensor components $\dot{\varepsilon}_{ij}$ according to following relationship:

$$\dot{\varepsilon}_i = \sqrt{\frac{2}{3}\dot{\varepsilon}_{ij}\dot{\varepsilon}_{ij}} \tag{7}$$

The components are given by (3). The second component of functional (5) is responding for friction. To compute friction power on the boundary S of area V a model given by the subsequent equation was used:

$$\dot{W}_t = \int_S m \frac{\sigma_p}{\sqrt{3}} \|\overline{\boldsymbol{v}}\| dS \tag{8}$$

In (8), m is the so called friction factor, which is usually experimentally selected and $\overline{\boldsymbol{v}}$ is a relative velocity vector of metal and tool $\overline{\boldsymbol{v}} = \boldsymbol{v} - \boldsymbol{v_t}$. In case of tensile test, the samples are permanently fixed in jaws of a physical simulator and friction must not be taken into account. However, compression test requires sharing the friction power which is significant.

For the solid zones the incompressibility condition can be described by universal operator equation independently of the mechanical state of the deformation process:

$$\nabla \mathbf{v} = 0 \tag{9}$$

Because the semi-solid zone is characterized by density change due to still ongoing progress of steel solidification, the condition of incompressibility is inadequate to reflect changes and was replaced with the mass conservation condition, which describes the following modified operational equation:

$$\nabla \mathbf{v} - \frac{1}{\rho}\frac{\partial \rho}{\partial t} = 0 \tag{10}$$

The basis for the optimization of functional (5) is the velocity field determined by appropriate system of velocity functions in the concerned area. These functions are then the source of deformation field and other physical quantities affecting the power functional formulation. Obtaining an accurate real velocity field requires the use of velocity functions depending on a number of variational parameters. The functions should be flexible enough to map the field throughout the whole volume of the deformation zone. Analytical description of each component of the velocity field with a single function in the whole area of deformation is not preferred. This approach creates difficulties especially in areas not subjected to the deformation where the velocity function should remain constant. Therefore, the solution to the problem of semi-solid metal flow was based on a specific method.

In the case of deformation of axial-symmetrical bodies, the incompressibility condition is given by following differential equation:

$$\frac{\partial v_r}{\partial r} + \frac{v_r}{r} + \frac{\partial v_z}{\partial z} = 0 \tag{11}$$

For the semi-solid area, (11) is replaced by the mass conservation condition due to existing density changes. The longitudinal velocity has been calculated as an analytical function of radial velocity using this condition. In cylindrical coordinate system the condition has been described with an equation:

$$\frac{\partial v_r}{\partial r} + \frac{v_r}{r} + \frac{\partial v_z}{\partial z} - \frac{1}{\rho}\frac{\partial \rho}{\partial \tau} = 0 \tag{12}$$

Equation (11) is a special case of (12) and therefore the proposed solution will consider the dependence (12) as more general. In (12) ρ is the temporary material density and τ is the time variable. The proposed variational formulation makes the longitudinal velocity dependent on the radial one. Condition (12) allows for the calculation of $\partial v_z/\partial z$ derivative as a function of $\partial v_r/\partial r$ after analytical differentiation of radial velocity distribution function $v_r(r,z)$. Hence, the longitudinal velocity is calculated as a result of analytical integration according to following equation:

$$v_z = -\int \left(\frac{\partial v_r}{\partial r} + \frac{v_r}{r} - \frac{1}{\rho}\frac{\partial \rho}{\partial \tau}\right) dz \tag{13}$$

2013, © Copyright by authors, Published under agreement with IARIA - www.iaria.org

In this case, the velocity field depends only on one function – the radial velocity distribution.

Heat exchange between solid metal and environment, and its flow inside the metal is controlled by a number of factors. During phase transformation two additional phenomena have to be taken into account. Note that in the process of deformation of steel at temperature of liquid to solid phase transformation there are two sources of heat changes. On the one hand, heat is generated due to the state transformation. On the other hand, it is secreted as a result of plastic deformation. In addition, steel density variations also cause changes of body temperature.

Thermal solution has a major impact on simulation results, since the temperature has strong effect on remaining variables. This is especially evident if the specimen temperature is close to solidus line when the body consist of both solid and semi-solid regions. In such case, the affected phenomena are: plastic flow of solid and mushy materials, stress evolution and density changes. The theoretical temperature field is a solution of Fourier-Kirchhoff equation with appropriate boundary conditions [16].

The most general form of the Fourier-Kirchhoff equation in any coordinate system can be written in operator form as follows:

$$\nabla^T(\mathbf{\Lambda}\,\nabla T) + Q = c_p\rho\left(\boldsymbol{v}^{\boldsymbol{T}}\nabla T + \frac{\partial T}{\partial \tau}\right) \tag{14}$$

where T is the temperature distribution in the controlled volume and $\mathbf{\Lambda}$ denotes the symmetrical second order tensor called heat transformation tensor. In case of thermal inhomogeneity, the whole tensor has to be considered. Q represents the rate of heat generation (or consumption) due to the phase transformation, due to plastic work done and due to electric current flow (resistance heating of the sample is usually applied). Finally, c_p describes the specific heat, ρ the steel density, $\boldsymbol{v}$ the velocity vector of specimen particles and τ the elapsed time.

For axial-symmetrical case, (14) can be simplified. The following form of Fourier-Kirchhoff equations for isotropic, axially-symmetric heat flow was applied in the presented solution:

$$\lambda\left(\frac{\partial^2 T}{\partial r^2} + \frac{1}{r}\frac{\partial T}{\partial r} + \frac{\partial^2 T}{\partial z^2}\right) + Q = \rho c_p\frac{\partial T}{\partial \tau} \tag{15}$$

Equation (15) needs to be solved with appropriate initial and boundary conditions. Combined Hankel's boundary conditions have been adopted for the presented model.

One of the most important parameters of the solution is the density. Its changes have influence on the mechanical part of the presented model. The knowledge of effective density distribution is very important for modelling the deformation of porous materials. Density changes of liquid, solid-liquid and solid materials are ruled over three phenomena: solid phase formation, laminar liquid flow through porous material and thermal shrinkage. Total density changes can be calculated according to following equation:

$$\frac{\partial \rho}{\partial \tau} = (\rho_s X_s + \rho_l X_l)\left(\frac{\partial_s}{\partial_l} - 1\right)\frac{\partial X_l}{\partial_\tau} + \rho_l X_l div\,\vartheta + (\beta_S\rho_S X_s + \beta_l\rho_l X_l)\frac{\partial T}{\partial \tau} \tag{16}$$

where X is the fraction and β the linear expansion coefficient. Indexes l and s denote the liquid and solid phases, respectively.

IV. Example Results - New Methodology Validation

The experimental work was done in Institute for Ferrous Metallurgy in Gliwice, Poland using Gleeble 3800 thermo-mechanical simulator (Figure 7).

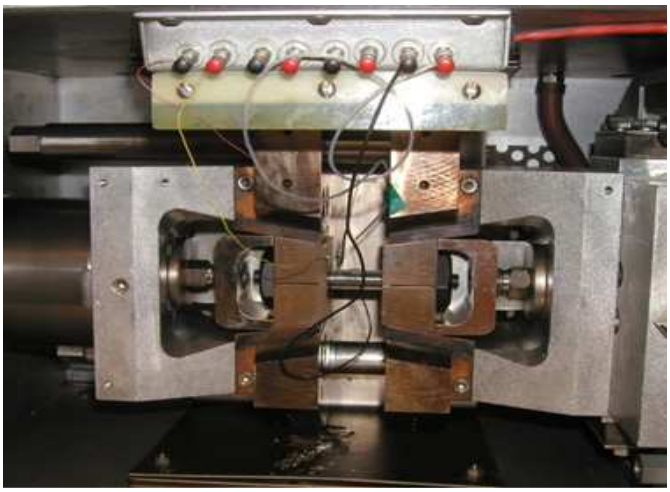

Figure 7. The standard Gleeble 3800 equipment allowing deformation is semi-solid state (right before running process).

The steel used for the experiments was the C45 grade steel having 0.45% of carbon content. In all cases, experiments were performed according to the following schedule:

- initial stage: sample preparation divided into several sub stages (e.g., thermocouple assembly); die selection, etc,
- stage 2: melting procedure,
- stage 3: deformation process.

It is good practice to test materials in isothermal conditions [11]. Unfortunately, this is not possible for semi-solid steel. Nevertheless, the condition should be as close to isothermal as possible due to the very high sensitivity of material rheology to even small variations of temperature. The basic reason for uneven temperature distribution inside the sample body on the Gleeble 3800 simulator is the contact with hot copper handles presented in Figure 8.

2013, © Copyright by authors, Published under agreement with IARIA - www.iaria.org

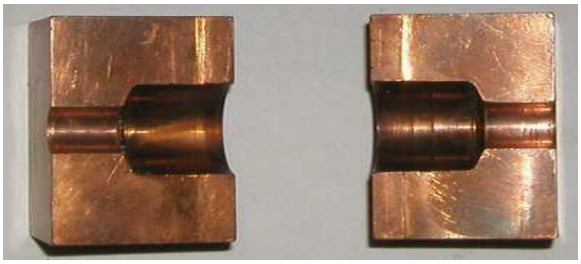

Figure 8. The short contact zone handles used in experiments (hot handle).

The estimated liquidus and solidus temperature levels of the investigated steel are: 1495°C and 1410°C, respectively. Thermal solution of the theoretical model has crucial influence on simulation results, since the temperature has strong effect on remaining parameters. The resistance sample heating and contact of the sample with cold cooper handles cause non-uniform distribution of temperature inside heated material, especially along the sample. The semi-solid conditions in central parts of the sample cause even greater temperature gradient due to latent heat of transformation. Such non-uniform temperature distribution is the source of significant differences in the microstructure and hence in material rheological properties.

During the experiments, samples were heated to 1430°C and after maintaining at constant temperature were cooled down to the required deformation temperature. In case of heating, the heat generated is usually not known because the Gleeble 3800 equipment uses an adaptive procedure for resistive heating controlled by temperature instead of current flow. Hence, the actual heat generated by current flow (in fact the rate of heat generation Q) has to be calculated using inverse procedure. In this case, the objective function (F) was defined as a norm of discrepancies between calculated (T_c) and measured (T_m) temperatures at a checkpoint (steering thermocouple position: TC4 in Figure 9) according to the following equation:

$$F(\mathrm{Q}) = \int_{\tau_0}^{\tau_i} [T_c(Q,r,z,T) - T_m(r,z,T)]d\tau \qquad (17)$$

where τ is the time variable, Q is the rate of heat generation.

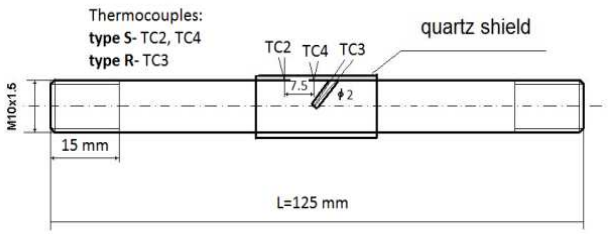

Figure 9. Samples used for the experiments. TC2, TC3 and TC4 thermocouples.

In the final stage of physical test, the temperature difference between core of the sample (TC3 thermocouple position) and its surface (TC4 thermocouple position) can be significant. In all cases the core temperature was higher than surface temperature. Differences between these two reach around 30°C for cold handle (handle with long contact zone) and about 40°C for hot handle. The results of numerical simulation are in agreement with experiments. In Figure 10 and Figure 11 the temperature distribution after 3 and 6 seconds of heating process are shown. One can observe increasing gradient of temperature near the die-sample interface.

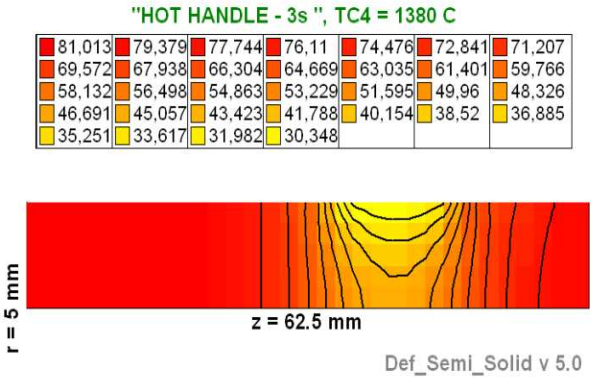

Figure 10. Temperature distribution after 3 seconds of heating.

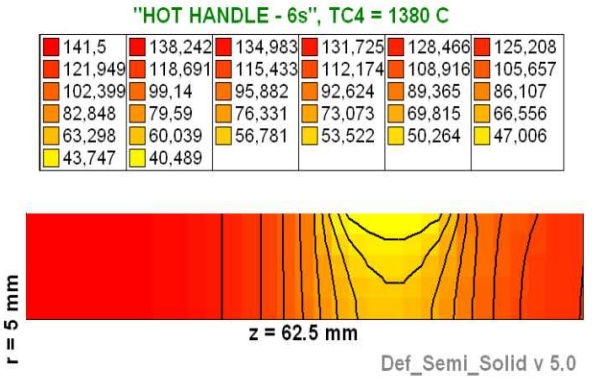

Figure 11. Temperature distribution after 6 seconds of heating.

Figure 12 presents the final temperature distributions in the cross section of sample tested at 1380°C right before deformation (variant with hot handle). One can observe major temperature gradient between die-sample contact surface (physical contact sample with tool). However, difference between experimental and theoretical core temperatures for hot handles was only 3°C (calculated core temperature was equal to 1417°C and measured one was equal to 1420°C).

2013, © Copyright by authors, Published under agreement with IARIA - www.iaria.org

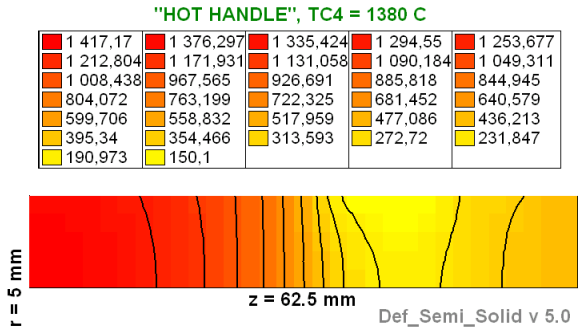

Figure 12. Distribution of temperature in the cross section of sample tested at temperature 1380°C right before deformation (variant with hot handle).

The micro and macrostructure of the tested samples were investigated as well. Figure 13 shows microstructure right before deformation for both central and boundary regions of the heating zone. Microstructure of the cooled samples consists of pearlite (the darkest phase), bainite (grey phase mainly near the borders of grains) and the bright ferrite. This is a result of phase composition, wide melting zone and almost two times lower rate of cooling of central parts of the sample (in the case of hot handles).

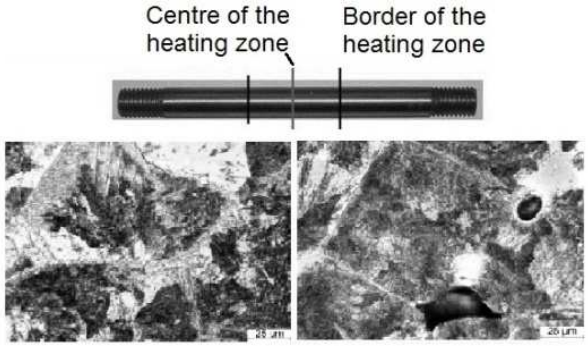

Figure 13. Microstructure of the central and boundary regions of sample right before deformation. Variant with cold handle. Magnification: 400x.

Figure 14 shows macrostructure of the central part of cross-sections of samples right before deformation. Liquid phase particles were observed. Experimental and numerical results can be compared taking into consideration the temperature gradient within the sample. This shows that the mathematical model of resistance heating is consistent with the experimental data.\

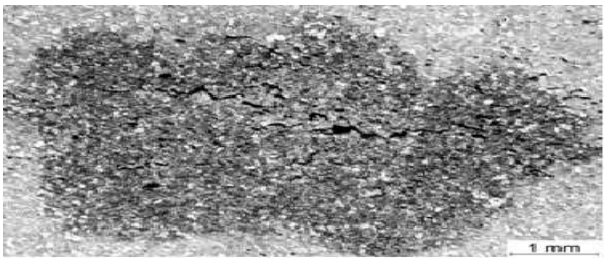

Figure 14. Macrostructure of the sample central part right before deformation. Variant with cold handle. Magnification: 10x.

Compression and tension tests were performed, according to the given methodology. During experiments die displacement, force and temperature changes in the deformation zone were recorded. The computer simulations were performed as well. All series of tests and computer simulations were done using long contact zone between samples and simulator jaws (cold handle). The deformation zone had the initial height of 62.5 mm. The sample diameter was 10 mm. The samples were melted at 1430°C and then cooled to deformation temperature. During the tests each sample was subjected to 10 mm reduction of height. Results of each test were used for inverse analysis to compute yield stress curve parameters. Figure 15 shows strain-stress curves at several strain rate levels for temperature 1300°C. The relationships were calculated using presented experimental methodology.

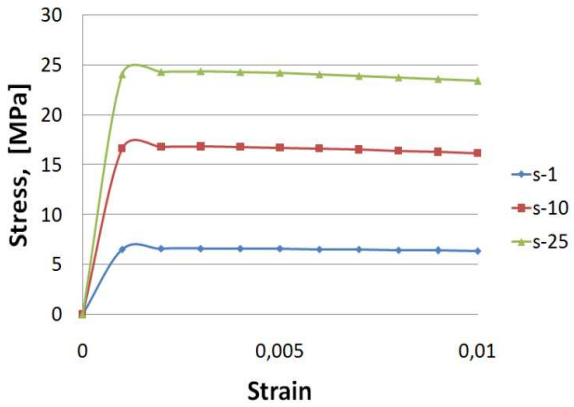

Figure 15. Stress-strain curves at several strain rate levels for temperature 1300°C.

Comparison between the calculated and measured loads are presented in Figure 16, showing quite good agreement.

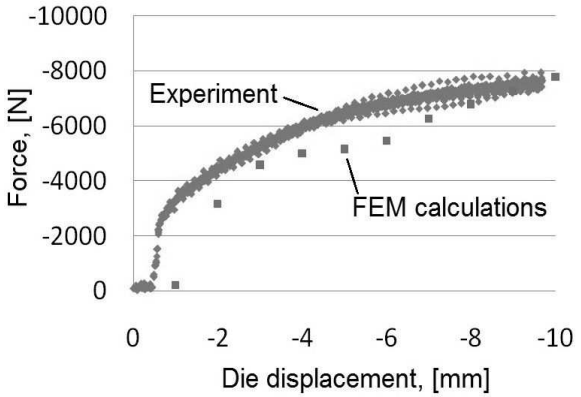

Figure 16. Comparison between measured and predicted loads at temperature 1380°C (new methodology).

Shape of a sample after experiment at 1300°C is presented in Figure 17.

2013, © Copyright by authors, Published under agreement with IARIA - www.iaria.org

Figure 17. Example final shape of the sample after deformation at 1300°C.

Comparison between the measured and calculated maximal diameters of samples allow rough verification of the developed computer aided experimental methodology. Results of such comparison are presented in Table 1. The table shows results for samples which have been subjected to deformation at several levels of temperature, i.e., 1300°C, 1350°C and 1380°C. Good agreement between the real diameter and its calculated value is observed. The relative mean square error between both the values is equal to 2.76%.

TABLE I. COMPARISION OF THE MEASURED AND CALCULATED MAXIMAL DIAMETERS OF SAMPLES DEFORMED AT DIFFERENT TEMPERATURE

Test	Experiment	Simulations
1300°C	15.3 mm	15.6 mm
1350°C	15.3 mm	15 mm
1380°C	17.8 mm	18.2 mm
Relative mean square error: 2.76%		

Figure 18 compares measured loads with those computed using the methodology previously used by the authors. One can see that the mean square error in this case is significantly greater than its equivalent for the newly developed method.

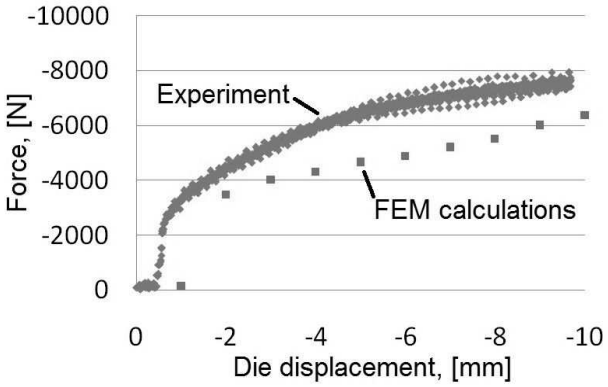

Figure 18. Comparison between measured and predicted loads at temperature 1380°C (old methodology).

The main reason for that is the lack of strain rate dependency of yield stress in the old model. The results obtained taking into account the strain rate as a parameter of the flow curve are more accurate for temperatures exceeding the NDT level.

V. EXAMPLE RESULTS OF INVESTIGATION OF 11SMN30 GRADE STEEL

In this section, the newest results of investigation of 11SMn30 grade steel are presented. The investigation procedures were analogous to those applied in case of C45 grade steel described in the previous chapter and based on new methodology. The long contact zone handles are used during all physical tests made using Gleeble 3800 thermo-mechanical simulator. The liquidus and solidus temperature of 11SMn30 grade steel are 1518°C and 1439°C, respectively. The average NST temperature for the selected steel was 1410±15°C. In order to determine the nil ductility temperature (NDT) a number of experiments were done. All the tests indicate a common temperature of 1425°C. The estimated ductility recovery temperature was 1400°C. At this temperature the sample's reduction of area was around 5% and rose very fast with the temperature drop. The predictions of strain-stress relationships were based on compression tests. The sample were melted at 1430°C and then deformed after dynamic cooling to selected temperature levels between 1200°C and NDT. The temperature program used for all experimental tests are presented in Figure 19.

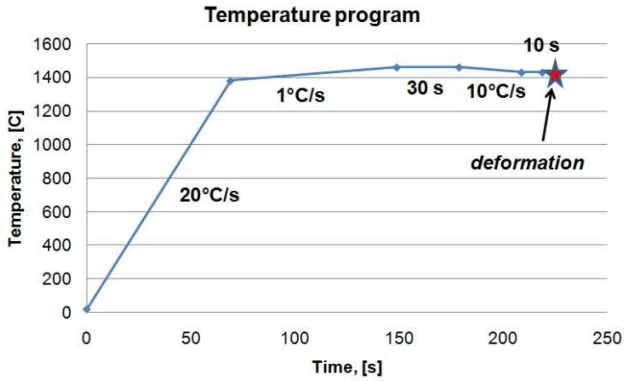

Figure 19. Temperature program used for all experimental tests.

For dynamic cooling and deformation processes in some regions of the sample the remainder of liquid phase can be observed at temperatures lower than NDT. We must remember that for cold handles the core temperature is higher about 35°C than nominal test temperature. Due to significant strain inhomogeneity inverse analysis is the only method allowing appropriate calculation of coefficients of yield stress functions at any temperature higher than NDT. The objective function was defined as a norm of discrepancies between calculated (F^c) and measured (F^m) loads in a number of subsequent stages of the compression according to the following equation:

$$\varphi(x) = \sum_{i=1}^{n} [F_i^c - F_i^m]^2 \qquad (18)$$

2013, © Copyright by authors, Published under agreement with IARIA - www.iaria.org

The theoretical forces F^c were calculated with the help of sophisticated FEM solver facilitating accurate computation of strain, stress and temperature fields for materials with variable density. As written before, experiments for temperatures higher than NDT are difficult. Several serious experimental problems arise. Apart from problems with keeping temperature constant and uniform during the whole experimental procedure there are also difficulties concerning interpretation of the measurement results. The inhomogeneity in strain distribution and distortion of the central part of the sample lead to poor accuracy of the stress fields calculated using traditional methods which are usually good for lower temperatures. Hence, the application of the developed FEM software is necessary in order to ensure appropriate interpretation of experimental data but experimental procedure has still to be carried out with great caution. More details concerning the applied inverse model can be found in [12].

Figure 20 presents an example graph of stress versus strain curve at temperature of 1400°C for the several strain rates levels. The presented curves are plotted using the calculated coefficients for temperature levels observed in the samples' cross-sections. The formula itself can be written in the following form:

$$\sigma_p = A\varepsilon^n \exp(B\varepsilon)\dot{\varepsilon}^m \exp(-CT) \qquad (19)$$

where: A, n, b, C are calculated coefficients and ε, $\dot{\varepsilon}$, T are strain, strain rate and temperature, respectively.

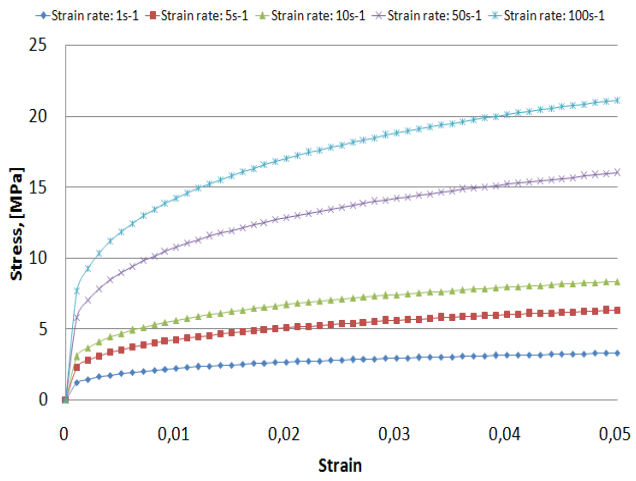

Figure 20. Flow stress vs strain at temperature 1400°C and several strain rate levels.

The comparison between the calculated and measured loads are presented in Figures 21-26, showing quite good agreement between both loads.

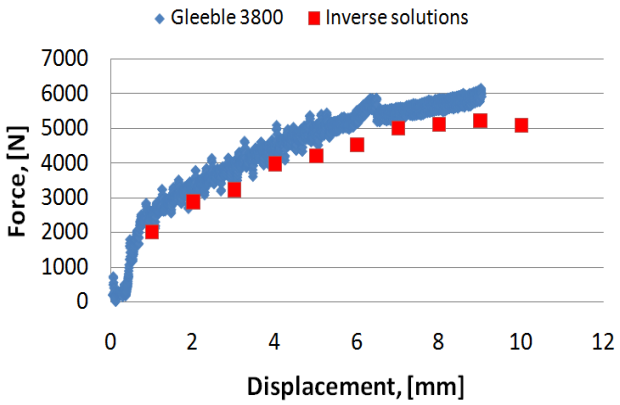

Figure 21. Comparison between measured and predicted loads at temperature 1350°C (medium-dynamic process).

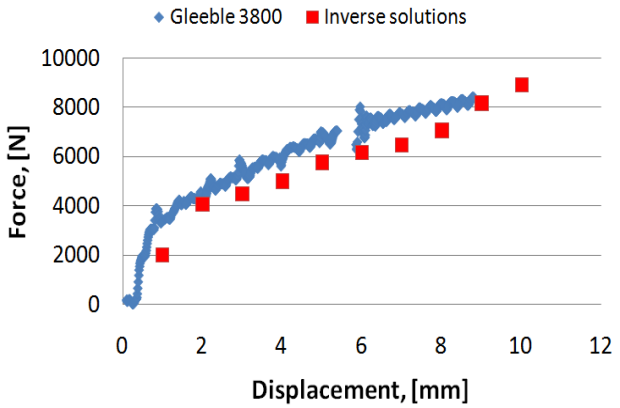

Figure 22. Comparison between measured and predicted loads at temperature 1350°C (high-dynamic process).

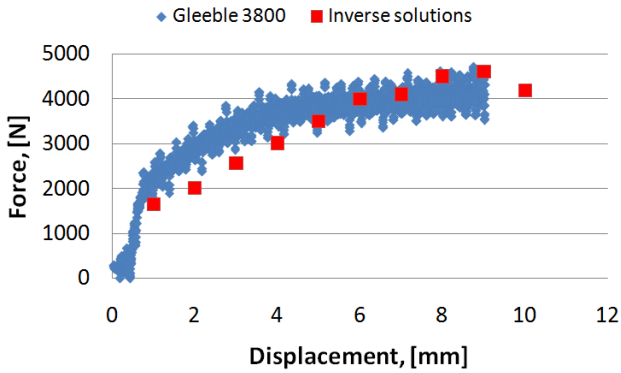

Figure 23. Comparison between measured and predicted loads at temperature 1400°C (medium-dynamic process).

2013, © Copyright by authors, Published under agreement with IARIA - www.iaria.org

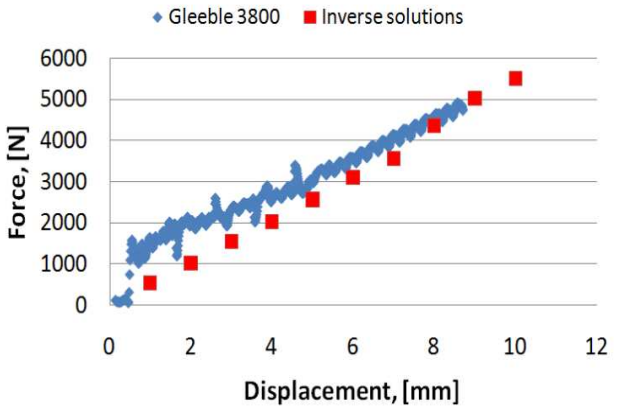

Figure 24. Comparison between measured and predicted loads at temperature 1400°C (high-dynamic process).

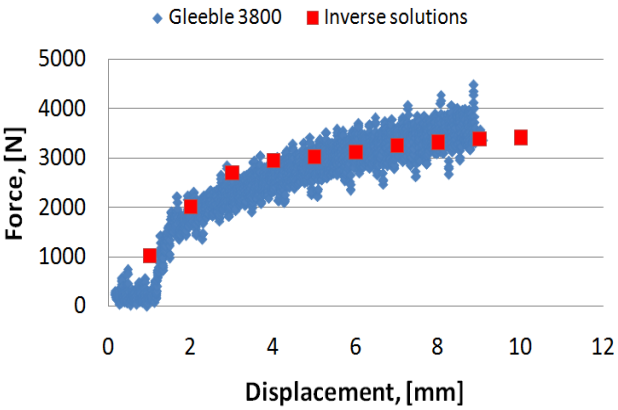

Figure 25. Comparison between measured and predicted loads at temperature 1420°C (medium-dynamic process).

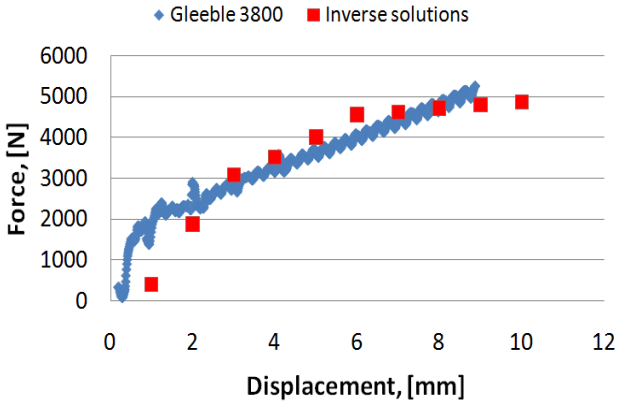

Figure 26. Comparison between measured and predicted loads at temperature 1420°C (high-dynamic process).

The verification of the model was done by comparing numerical and experimental results. The developed yield stress curves were used for example simulations of compression of cylindrical samples with mushy central part. The length of the potential deformation zone of the sample was 30 mm (the rest was mounted in the testing equipment jaws), but only a part of it has been subjected to the deformation due to huge temperature gradient along the sample. Samples were melted at 1430°C and then subjected to the deformation at nominal test temperature with height reduction of 10 mm. In Figure 27, the final temperature distribution in the cross-section of the sample just before the deformation at 1425°C is presented. Taking into account the value of NDT temperature, solidus temperature as well as the temperature difference between the surface and central part of the sample one can assume existence of mushy zone in the sample volume.

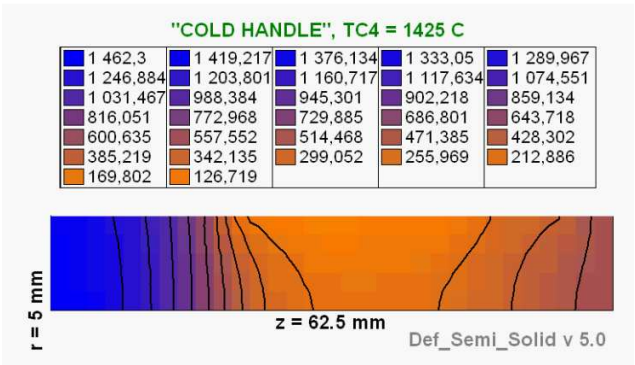

Figure 27. Initial temperature distribution (right before the deformation at 1425°C) in the ¼ part of sample cross-section.

The non-uniform temperature distribution in the sample cross-section has a great influence on the strain field and deformation zone size and shape. The inhomogeneity of the strain field leads to inhomogeneous stress distribution. The analysis of the strain shows its maximum values in the central region of the sample. In the Figures 28-33, example strain distribution in the cross section of the deformed samples at several temperatures are presented. The one can observe that strain level is higher for high-dynamic process. On the other hand, the level of strain increases with increasing test temperature for both processes: medium and high-dynamic.

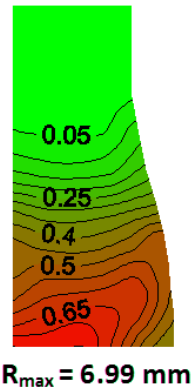

Figure 28. Strain distribution in the ¼ cross-section of the sample deformed at 1350°C for the medium-dynamic process.

2013, © Copyright by authors, Published under agreement with IARIA - www.iaria.org

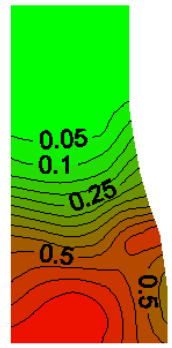

Figure 29. Strain distribution in the ¼ cross-section of the sample deformed at 1400°C for the medium-dynamic process.

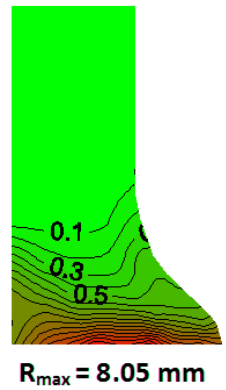

Figure 30. Strain distribution in the ¼ cross-section of the sample deformed at 1420°C for the medium-dynamic process.

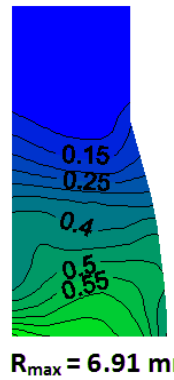

Figure 31. Strain distribution in the ¼ cross-section of the sample deformed at 1350°C for the high-dynamic process.

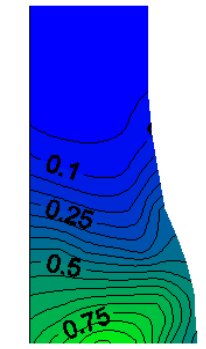

Figure 32. Strain distribution in the ¼ cross-section of the sample deformed at 1400°C for the high-dynamic process.

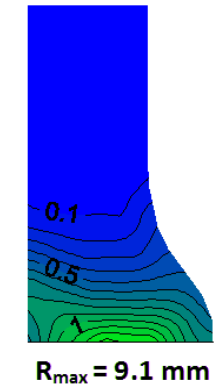

Figure 33. Strain distribution in the ¼ cross-section of the sample deformed at 1420°C for the high-dynamic process.

Example shape of a sample after experiment at 1420°C is presented in Figure 34. Visible cracks formed during virtually all attempts carried out in the temperature ranges close NDT temperature. The proposed mathematical model of steel deformation in semi-solid state does not take into account this phenomena. The authors have run further investigations leading to development of crack propagation model, which will be implemented into developed FEM system.

Figure 34. Example final shape of the sample after deformation at 1420°C with visible crack propagation (medium-dynamic process).

2013, © Copyright by authors, Published under agreement with IARIA - www.iaria.org

Finally, the verifications of the model were done. Two main comparative criteria were used for the verification:
-comparison between the measured and calculated maximum sample radii,
-comparison between the measured and calculated length of zone, which is not subjected to the deformation.
Figures 35-36 and Figures 37-38 show example application of the 1st and 2nd criterion, respectively. The figures confirm quite good agreement between theoretical and experimental results.

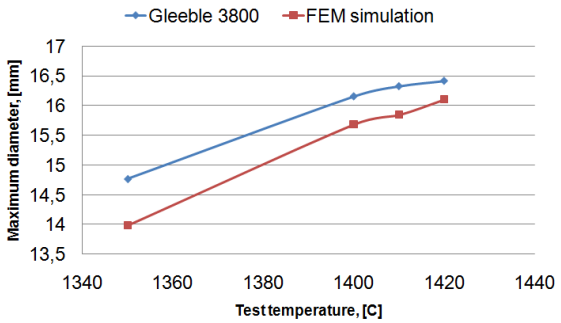

Figure 35. The comparison of the measured and calculated maximum diameters of the sample – deformation in temperature range 1350°C to 1420°C (medium-dynamic process).

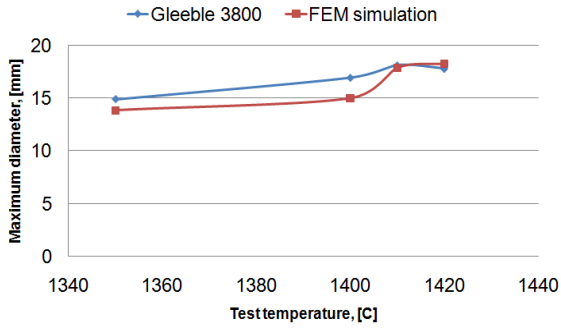

Figure 36. The comparison of the measured and calculated maximum diameters of the sample – deformation in temperature range 1350°C to 1420°C (high-dynamic process).

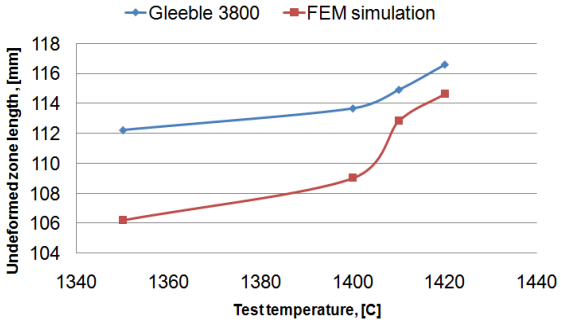

Figure 37. The comparison of the measured and calculated length of zone, which was not subjected to the deformation – experiment in temperature range 1350°C to 1420°C (medium-dynamic process).

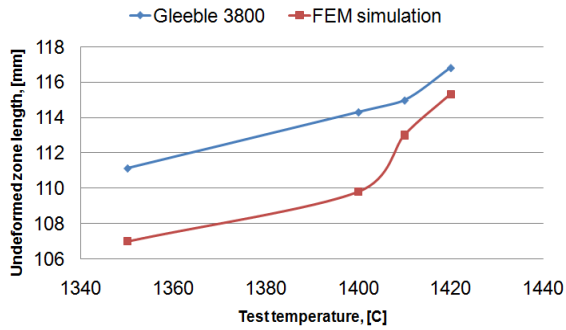

Figure 38. The comparison of the measured and calculated length of zone, which was not subjected to the deformation – experiment in temperature range 1350°C to 1420°C (high-dynamic process).

VI. Conclusion And Future Work

The investigations reported in the current paper have shown that temperature distribution inside the controlled semi-solid volume is strongly heterogeneous and non-uniform. Axial-symmetrical model does not take into account all the physical phenomena accompanying the deformation. Finally, the error of the predicted strain-stress curves can still be improved. The proposed solution of the presented problem is application of both fully three-dimensional solution and more adequate solidification model taking into consideration evolution of forming steel microstructure. Therefore, the study of multiscale modelling of mechanical properties is the main target of the future work. Contrary to the current model, the new approach should allow to better capture the physical principles of semi-solid steel deformation in micro-scale. Additionally, the methodology should allow to transfer the characteristics of the material behaviour between the micro- and macro-scale. As a consequence, the final results should be more precise and accurate. Modelling of deformation of steel samples at extra-high temperatures involves a number of issues. One of them is the difficulty of calculating of thermal and mechanical material properties. Another most important problem is the right interpretation of the results of compression tests that provide data for flow stress calculation. The presented testing methodology allows reliable numerical simulation of deformation of semi-solid steel samples and calculation of realistic flow curve parameters. The presented research was focused on mechanical properties of investigated semi-solid steel. Compression tests carried out for semi-solid materials could only be interpreted using inverse analysis. Temperature strain and strain rate as parameters of the flow curve provide accurate results of computer simulation of semi-solid steel behaviour.

The authors have run further investigations leading to development of fully three-dimensional simulation system of integrated casting and rolling processes, as well as the soft reduction process, that are part of strip casting technology. Like the model presented in the hereby paper,

2013, © Copyright by authors, Published under agreement with IARIA - www.iaria.org

the spatial one focus on three main aspects: thermal, mechanical and density changes. All of them are dependent on each other

ACKNOWLEDGMENT

The project has been supported by the Polish National Science Centre, Decision number: DEC-2011/03/D/ST8/04041

REFERENCES

[1] M. Glowacki and M. Hojny, "Computer-aided investigation of mechanical properties for integrated casting and rolling processes using hybrid numerical-analytical model of mushy steel deformation," in Proceedings of the Sixth International Conference on Advanced Engineering Computing and Applications in Sciences (ADVCOMP 2012), 2012.

[2] D. Senk, F. Hagemann, B. Hammer, and R. Kopp, “Umformen und Kühlen von direkt gegossenem,” Stahlband, Stahl und Eisen, vol. 120, 2000, pp. 65-69.

[3] H.G. Suzuki and S. Nishimura, “Physical simulation of the continuous casting of steels,” Proceedings of Physical Simulation of Welding, Hot Forming and Continuous Casting, Canmet Canada, May 2-4, 1988, pp. 166-191.

[4] A. Gołdasz, Z. Malinowski, and B. Hadała, " Study of heat balance in the rolling process of bars," Archives of Metallurgy and Materials, vol. 54, 2009, pp. 685–694.

[5] T. Telejko, Z. Malinowski, and M. Rywotycki, " Analysis of heat transfer and fluid flow in continuous steel casting," Archives of Metallurgy and Materials, vol. 54, 2009, pp. 837–844.

[6] R. Kopp, J. Choi, and D. Neudenberger, "Simple compression test and simulation of an Sn–15% Pb alloy in the semi-solid state," J. Mater. Proc. Technol.,vol. 135, 2003, pp. 317-323, doi: 10.1016/S0924-0136(02)00863-4.

[7] M. Modigell, L. Pape, and M. Hufschmidt,"The Rheological Behaviour of Metallic Suspensions," Steel Research Int., vol. 75, 2004, pp. 506–512.

[8] Y.L. Jing, S. Sumio, and Y. Jun, "Microstructural evolution and flow stress of semi-solid type 304 stainless steel," J. Mater. Proc. Technol., vol. 161, 2005, pp. 396–406, doi: 10.1016/j.jmatprotec.2004.07.063.

[9] M. Hojny, "Application of an integrated CAD/CAM/CAE/IBC system in the stamping process of a bathtub 1200 S," Archives of Metallurgy and Materials, vol. 55, 2010, pp. 713–723.

[10] M. Paćko, M. Dukat, T. Śleboda, and M. Hojny ,"The analysis of multistage deep drawing of AA5754 aluminum alloy," Archives of Metallurgy and Materials, vol. 55, 2010, pp. 1173–1184. DOI: 10.2478/v10172-010-0021-5.

[11] M. Hojny and M. Glowacki," Computer modelling of deformation of steel samples with mushy zone," Steel Research Int., vol. 79, 2008, pp. 868-874. DOI: 10.2374/SRI08SP083.

[12] M. Głowacki and M. Hojny,"Inverse analysis applied for determination of strain-stress curves for steel deformed in semi-solid state," Inverse Problems in Science and Engineering, vol. 17, 2009, pp.159–174. DOI: 10.1080/17415970802082757.

[13] M. Hojny and M. Glowacki, "The methodology of strain – stress curves determination for steel in semi-solid state," Archives of Metallurgy and Materials, vol. 54, 2009, pp. 475–483.

[14] M. Hojny and M. Glowacki, "The physical and computer modeling of plastic deformation of low carbon steel in semi-solid state," Journal of Engineering Materials and Technology, vol. 131, 2009, pp. 041003.1-041003.7, DOI: 10.1115/1.3184034.

[15] M Hojny and M. Głowacki ,"Computer aided methodology of strain-stress curve construction for steels deformed at extra high temperature," High Temperature Materials and Processes, vol. 28, 2009, pp. 245–252. DOI: 10.1515/HTMP.2009.28.4.245.

[16] M. Hojny and M. Glowacki, "Modeling of strain-stress relationship for carbon steel deformed at temperature exceeding hot rolling range," Journal of Engineering Materials and Technology, vol. 133, 2011, pp. 021008.1-021008.7, DOI: 10.1115/1.4003106.

2013, © Copyright by authors, Published under agreement with IARIA - www.iaria.org